Polymer 126 (2017) 283–290

Contents lists available at ScienceDirect

Polymer

journal homepage: www.elsevier.com/locate/polymer

Structure-property relationships for covalent triazine-based frameworks: The effect of spacer length on photocatalytic hydrogen evolution from water

Christian B. Meier [a], Reiner Sebastian Sprick [a], Adriano Monti [b], Pierre Guiglion [b], Jet-Sing M. Lee [a], Martijn A. Zwijnenburg [b], Andrew I. Cooper [a, *]

[a] Department of Chemistry and Materials Innovation Factory, University of Liverpool, Crown Street, Liverpool, L69 7ZD, United Kingdom
[b] Department of Chemistry, University College London, 20 Gordon Street, London WC1H 0AJ, United Kingdom

ARTICLE INFO

Article history:
Received 9 January 2017
Received in revised form
3 April 2017
Accepted 5 April 2017
Available online 6 April 2017

Keywords:
Photocatalysis
Hydrogen evolution from water
Covalent triazine-based framework (CTF)

ABSTRACT

Covalent triazine-based frameworks (CTFs) are a subclass of conjugated microporous polymers (CMPs) that can be used as organic photocatalysts for photocatalytic hydrogen evolution from water. Seven materials with varied spacer units from phenylene to quarterphenylene were synthesized, either by trifluoromethanesulfonic acid (TfOH) catalysis from nitriles or by Suzuki-Miyaura polycondensation. The photocatalytic performance under visible light of all materials was systematically studied in the presence of a hole-scavenger, showing that both synthesis routes produce CTFs with similar hydrogen evolution rates (HER), but different optical properties. The highest hydrogen evolution rate in the cyclotrimerized series was found for CTF-2 with an apparent quantum yield of 1.6% at 420 nm in a mixture of water and triethanolamine with a platinum co-catalyst. Based on (TD-)DFT calculations, the highest performance was expected for CTF-1 and this discrepancy is explained by a trade-off between increased light absorption and decreased thermodynamic driving force.

1. Introduction

Until recently, direct photocatalytic hydrogen production using particulate photocatalysts has been dominated by inorganic materials [1–3], but there is now a growing interest in organic and polymeric photocatalysts [4]. Graphitic carbon nitride (g-C_3N_4) is the most extensively studied material in this class for hydrogen evolution from water [5–10] and it has been reported to drive overall water splitting *via* a four-electron pathway [11,12]. One of the drawbacks of graphitic carbon nitride is the limited scope for fine-tuning the structure and properties as the synthesis is carried out at temperatures above 520 °C [9]. Materials are typically modified by varying the nitrogen rich starting materials [13,14] or by doping methods; for example, by adding sulfur [15] or potassium hydroxide [16]. This difficulty in tailoring the photophysical properties of g-C_3N_4 makes it attractive to study polymeric organic photocatalysts, which can be synthesized by coupling a diverse range of monomers at low temperatures, thus allowing fine synthetic control over the primary structure. Poly(*p*-phenylene)s [17,18], oligo(*p*-phenylene)s [19] and poly(pyridine-2,5-diyl) [20] show limited catalytic activity for hydrogen evolution from water in the presence of a sacrificial hole-scavenger, mostly under UV light. More recently, conjugated microporous polymer (CMP) photocatalysts synthesized by Suzuki-Miyaura polycondensation of substituted pyrenes and benzenes [21,22] have shown promising photocatalytic activities, and the absorption spectrum can be shifted into the visible region by varying the co-monomer composition. A further study on CMPs [23] explored the influence of substitution patterns and conjugation lengths on the hydrogen evolution rates. CMPs based on 4,8-di(thiophen-2-yl)benzo[1,2-*b*:4,5-*b*′]dithiophene [24,25] have also shown good activity. Besides these CMPs, linear conjugated *co*-polymers of planar units were shown to have even higher activities for photocatalytic hydrogen evolution in the presence of triethylamine as sacrificial hole-scavenger [26]. Subsequently, poly(phenyl-*co*-benzothiadiazole)s [27] and poly(fluorene-*co*-benzothiadiazole) [28] were both shown to promote hydrogen evolution from water in the presence of sacrificial hole-scavengers.

Covalent triazine-based frameworks (CTFs) have also been studied for photocatalytic hydrogen evolution from water. CTFs are

* Corresponding author.
E-mail address: aicooper@liverpool.ac.uk (A.I. Cooper).

http://dx.doi.org/10.1016/j.polymer.2017.04.017

similar to g-C_3N_4 in terms of their high nitrogen content and their synthesis which often, but not always, involves ionothermal approaches in molten salt or molten eutectic salt mixtures with temperatures over 350 °C [29–32]. CTFs for photocatalysis were prepared previously by condensation of 1,3,5-tris(4-formyl-phenyl) triazine and 2,5-diethyoxy-terephthalohydrazide to form hydrazones at 120 °C *via* microwave synthesis [33] and also obtained by a thermal azine formation form 4,4′,4″-(1,3,5-triazine-2,4,6-triyl)tris [benzaldehyde] and hydrazine at 120 °C [34]. Other CTF photocatalysts were synthesized by acid catalyzed, low temperature trimerizations of nitrile precursors, such as tetra(4-cyanophenyl) ethylene (25 °C) [35], terephtalonitrile and methylterephthalonitrile (0 °C) [36].

In this study, we prepared a range of structurally related CTFs using low temperature synthesis routes and explored the effect of structure and synthesis conditions on photocatalytic hydrogen evolution under sacrificial conditions.

2. Methods

All reagents were obtained from Sigma-Aldrich or from Alfa Aesar and used as received, except for [1,1′:4′,1″-terphenyl]-4,4″-dicarbonitrile (M3) and [1,1′:4′,1″:4″,1‴-quaterphenyl]-4,4‴-dicarbonitrile (M4), which were synthesized according to literature procedures [37,38]. 2,4,6-Tris(4-bromophenyl)-1,3,5-triazine (M5) was synthesized *via* acid catalyzed trimerization and 2,4,6-tris-[4-(4,4,5,5-tetramethyl-1,3,2-dioxaborolan-2-yl)phenyl]-1,3,5-triazine (M6) was synthesized using a modified Miyaura-borylation protocol [21]. Water for the hydrogen evolution experiments was purified using an ELGA LabWater system with a Purelab Option S filtration and ion exchange column ($\rho = 15$ MΩ cm) without pH level adjustment. Reactions were carried out under nitrogen atmosphere using standard Schlenk techniques. CHN Analysis was performed on a Thermo EA1112 Flash CHNS-O Analyzer using standard microanalytical procedures. The UV-visible absorption spectra of the polymers were recorded on a Shimadzu UV-2550 UV-Vis spectrometer as powders in the solid state. The ball milled polymer powders were prepared by grinding the polymer samples in a Retsch 400 MM mixer mill at a frequency of 30 Hz for 30 min. The mixer mill was equipped with 10 mL stainless steel grinding jars that contained two stainless steel grinding balls with a diameter of 7 mm. (TD-)DFT calculations were performed using the Turbomole 6.6 code [39], the B3LYP [40,41] density functional and the COSMO solvation model [42], for more details see the supporting information.

2.1. Hydrogen evolution experiments

A flask was charged with the polymer powder (25 mg), water (20.0 mL), triethanolamine (5.0 mL), H_2PtCl_6 solution (0.02 mL, 8 wt % in H_2O) or with the polymer powder (25 mg), water (20.0 mL), triethylamine (2.5 mL), methanol (2.5 mL), H_2PtCl_6 solution (0.02 mL, 8 wt % in H_2O) and sealed with a septum. The resulting suspension was ultra-sonicated for 10 min until the photocatalyst was well dispersed before degassing by N_2 bubbling for 30 min. The reaction mixture was side-illuminated with a 300 W Newport Xe light-source (Model: 6258, Ozone free) for the time specified. The lamp was cooled and IR light cut out by water circulating through a metal jacket with quartz windows. Gas samples were analyzed with a Bruker gas chromatograph.

2.2. General procedure for the acid catalyzed trimerization polymerization

Trifluoromethanesulfonic acid and $CHCl_3$ were added to a flask under nitrogen and the monomer dissolved in chloroform was added with a syringe pump at a rate of 2 ml min^{-1}. The reaction was stirred for 48 h before it was poured onto an aqueous ammonia solution (28.0–30.0% NH_3 basis) to neutralize the trifluoromethanesulfonic acid. The suspension was left stirring for 1 h after the addition of the ammonia solution. The resulting solid was filtered, washed successively with dichloromethane, ethanol, water and methanol. The samples were dried under vacuum at 75 °C overnight to obtain the polymer.

2.2.1. CTF-1

Trifluoromethanesulfonic acid (2.83 mL, 32.0 mmol), $CHCl_3$ (5.00 mL) and 1,4-dicyanobenzene (513 mg, 4.00 mmol) in 40 mL $CHCl_3$ were used in the polymerization. After the addition of the monomer, the solution was heated to 50 °C for 1 day, cooled to room temperature and continued with the general procedure. After work-up, the product was obtained as a white powder (328 mg) in 63% yield. Calc. for $(C_4H_2N)_n$: C, 74.99; H, 3.15; N, 21.86%; Found: C, 57.71; H, 3.72; N, 15.88%.

2.2.2. CTF-2

Trifluoromethanesulfonic acid (2.83 mL, 32.0 mmol), $CHCl_3$ (5.00 mL) and 4,4′-biphenyldicarbonitrile (817 mg, 4.00 mmol) in 40 mL $CHCl_3$ were used in the polymerization. After work-up, the product was obtained as a pale yellow powder (600 mg) in 73% yield. Calc. for $(C_7H_4N)_n$: C, 82.33; H, 3.95; N, 13.72%; Found: C, 75.88; H, 3.81; N, 12.21%; Found for the ball milled sample C, 75.62; H, 3.81; N, 12.17%.

2.2.3. CTF-3

Trifluoromethanesulfonic acid (0.40 mL, 4.48 mmol), $CHCl_3$ (0.10 mL) and [1,1′:4′,1″-terphenyl]-4,4″-dicarbonitrile (157 mg, 560 μmol) in 0.56 mL $CHCl_3$ were used in the polymerization. After work-up, the product was obtained as a pale green powder (110 mg) in 70% yield. Calc. for $(C_{10}H_6N)_n$: C, 85.69; H, 4.31; N, 9.99%; Found: C, 81.54; H, 4.57; N, 8.90%.

2.2.4. CTF-4

Trifluoromethanesulfonic acid (0.40 mL, 4.48 mmol), $CHCl_3$ (0.10 mL) and [1,1′:4′,1″:4″,1‴-quarter-phenyl]-4,4‴-dicarbonitrile (200 mg, 560 μmol) in 0.56 mL $CHCl_3$ were used in the polymerization. After work-up, the product was obtained as a pale green powder (164 mg) in 82% yield. Calc. for $(C_{13}H_8N)_n$: C, 87.62; H, 4.52; N, 7.86%; Found: C, 82.39; H, 4.47; N, 7.55%.

2.3. General procedure for the Pd(0)-catalyzed Suzuki-Miyaura polycondensation

The flask was charged with the monomers, *N,N*-dimethylformamide, an aqueous solution of K_2CO_3 (2.0 M) and degassed by bubbling with N_2 for 30 min [$Pd(PPh_3)_4$] (1.2 mol %) was added and the solution was degassed by bubbling with N_2 for 10 min before heated to 150 °C for 48 h. The mixture was cooled to room temperature and poured into water. The precipitate was collected by filtration and washed with H_2O and methanol. Further purification of the polymer was carried out by Soxhlet extraction with cyclopentyl methyl ether for two days and the product was dried under reduced pressure at 125 °C.

2.3.1. CTF-2 Suzuki

2,4,6-Tris[4-(4,4,5,5-tetramethyl-1,3,2-dioxaborolan-2-yl) phenyl]-1,3,5-triazine (500 mg, 728 μmol), 2,4,6-tris(4-bromophenyl)-1,3,5-triazine (397 mg, 728 μmol), *N,N*-dimethylformamide (10.9 mL), aqueous K_2CO_3 (2.0 M, 2.18 mL) and [$Pd(PPh_3)_4$] (10.1 mg, 1.2 mol %) were used in the polymerization.

After work-up, the product was obtained as a pale yellow powder (440 mg) in 98% yield. Calc. for $(C_7H_4N)_n$: C, 82.33; H, 3.95; N, 13.72%; Found: C, 69.26; H, 4.84; N 9.00%.

2.3.2. CTF-3 Suzuki

1,4-Benzene diboronic acid (182 mg, 1.10 mmol), 2,4,6-tris(4-bromophenyl)-1,3,5-triazine (400 mg, 733 μmol) *N,N*-dimethylformamide (16.5 mL), aqueous K_2CO_3 (2.0 M, 3.3 mL) and $[Pd(PPh_3)_4]$ (15 mg, 1.2 mol %) were used in the polymerization. After work-up, the product was obtained as a pale green powder (225 mg) in 73% yield. Calc. for $(C_{10}H_6N)_n$: C, 85.69; H, 4.31; N, 9.99%; Found: C, 79.60; H, 4.49; N 8.97%.

2.3.3. CTF-4 Suzuki

4,4′-Biphenyldiboronic acid bis(pinacol) ester (71.7 mg, 177 μmol), 2,4,6-tris(4-bromophenyl)-1,3,5-triazine (64.3 mg, 118 μmol) *N,N*-dimethylformamide (2.65 mL), aqueous K_2CO_3 (2.0 M, 0.53 mL) and $[Pd(PPh_3)_4]$ (2.40 mg, 1.2 mol %) were used in the polymerization. After work-up, the product was obtained as a pale green powder (44.9 mg) in 71% yield. Calc. for $(C_{13}H_8N)_n$: C, 87.62; H, 4.52; N, 7.86%; Found: C, 67.89; H, 3.89; N 6.12%.

3. Results and discussion

We present here a series of CTFs and compare the influence of the phenylene spacer length and the synthesis methods on the photocatalytic hydrogen evolution rate. We further compare the measured properties of these materials with theoretical (TD-)DFT predictions.

Two series of CTFs were synthesized (Fig. 1). CTF-1 to CTF-4 were obtained by acid catalysis and CTF-2 Suzuki to CTF-4 Suzuki were made using palladium chemistry. The numerals in these names refer to the length of the *para*-phenylene spacers between the triazines in the material (*i.e.*, CTF-1 = phenyl, CTF-2 = biphenyl, etc). CTF-1 to CTF-4 were synthesized *via* trifluoromethanesulfonic acid (TfOH) catalyzed cyclotrimerization of the corresponding dicyano arenes [43]. The reaction proceeded well at ambient temperature for 4,4′-biphenyl-dicarbonitrile (M2), [1,1′:4′,1″-terphenyl]-4,4″-dicarbonitrile (M3) and [1,1′:4′,1″:4″,1‴-quaterphenyl]-4,4‴-dicarbonitrile (M4). However, in the case of 4,4′-dicyano benzene (M1) [36], it was necessary to increase the reaction temperature to 50 °C.

CTF-2 Suzuki to CTF-4 Suzuki were prepared *via* palladium(0)-catalyzed Suzuki-Miyaura type polycondensation of 2,4,6-tris(4-bromophenyl)-1,3,5-triazine (M5) and 2,4,6-tris-[4-(4,4,5,5-tetramethyl-1,3,2-dioxaborolan-2-yl)phenyl]-1,3,5-triazine (M6), 1,4-benzene diboronic acid (M7), or 4,4′-biphenyldiboronic acid bis(pinacol) ester (M8) in *N,N*-dimethylformamide (DMF) at 150 °C in the presence of aqueous K_2CO_3. For both sets of materials, the polymers were obtained as powders and ball milled prior to analysis and photocatalysis experiments.

All CTFs were insoluble in common organic solvents tested (*i.e.*, acetone, methanol, hexane, dichloromethane, toluene, tetrahydrofuran, and *N,N*-dimethylformamide). Fourier-transform infrared spectroscopy (FT-IR) shows a significant decrease in intensity for the aryl nitrile band around 2230–2220 cm^{-1} compared to the monomer for the TfOH catalyzed series (CTF-1 to CTF-4), qualitatively indicating a high degree of polymerization (Fig. S-1, ESI). The FT-IR spectra of the Suzuki-coupled polymers show similar features compared to those prepared by TfOH catalysis, except for the expected absence of a nitrile band. Even though no distinct features in the FT-IR can be assigned to hydrolysis products, partial hydrolysis of unreacted nitrile groups at the end of the polymerization or during work-up in polymers CTF1, CTF-2, and CTF-4 is conceivable. All polymers are porous to nitrogen at 77 K after ball milling, except CTF-1 and CTF-4. CTF-2 shows the highest apparent Brunauer-Emmett-Teller surface area (SA_{BET}) of 560 $m^2\ g^{-1}$, while all others have SA_{BET} in the range from 200 to 400 $m^2\ g^{-1}$. Polymers CTF-1 and CTF-2 were reported previously to have similar FT-IR spectra and surface areas [43]. The polymers also show moderate gas uptakes for H_2, CO_2, Kr, and Xe (Table S-1, ESI), with CTF-2 showing the highest uptakes for H_2 (5.35 mmol g^{-1} at 77 K, 1 bar), CO_2 (1.25 mmol g^{-1} at 298 K, 1 bar), Kr (0.45 mmol g^{-1} at 298 K, 0.9 bar), and Xe 1.73 mmol g^{-1} (298 K, 1 bar). Powder X-ray diffraction patterns were featureless, indicating that both synthesis routes result in amorphous materials without any long-range order (Fig. S-7, ESI). This is probably due to the irreversible nature of the low temperature synthesis routes employed, since dynamic bond formation is believed to be necessary to give crystalline materials [44,45]. By contrast, limited crystallinity in CTFs has been reported for materials synthesized using ionothermal [29,30] and microwave routes [43]. Residual palladium was determined *via* ICP-OES and found to be 0.27 wt % for CTF-2 Suzuki, 0.07 wt % for CTF-3 Suzuki, and 0.65 wt % for CTF-4 Suzuki (Fig. S-28 and Table S-3, ESI). Energy-dispersive X-ray spectroscopy also confirms that residual palladium is present in the materials synthesized *via* Suzuki-Miyaura coupling (Table S-4, ESI). Thermogravimetric analysis (TGA) shows that the materials are stable up to 300 °C (Fig. S-2, ESI), except for CTF-1 which has a decomposition onset of 265 °C, possibly indicating a lower degree of polycondensation. Comparing both series of materials, the materials synthesized *via* TfOH trimerization show an earlier decomposition on-set compared to the polymers made by Suzuki coupling. This could be due to lower molecular weight of the polymers, which might also affect the photo-physical properties (*infra vide*). In contrast to previous reports [36,43], we found that when CTF-1 was synthesized at room temperature, the onset of decomposition was even lower (245 °C; Fig. S-3, ESI) and a photocatalytically inactive material was obtained. The samples were isolated after work-up as macroscopic particles (CTF-1, CTF-2 Suzuki, CTF-3 Suzuki, CTF-4 and CTF-4 Suzuki) or as macroscopic flakes (CTF-2 and CTF-3). After ball milling, SEM images of all materials (Fig. S-30–S-33, ESI) were obtained to estimate the decrease in particle size. The particle size of CTF-1 could be reduced from around 100 μm–10 μm. The average particle size of CTF-2, CTF-3, CTF-2 Suzuki and CTF-3 Suzuki were decreased from several millimeters to smaller particles in the range of a few hundred micrometers. By contrast, the particle size of CTF-4 and CTF-4 Suzuki was not decreased after ball milling, probably due to the softness and lower density of the networks.

UV-visible spectra (Fig. 2) show that the optical gap of the polymer depends on the length of the 1,4-phenylene linker between the triazine cores. Within the series CTF-1–CTF-4, the optical gap decreases from 2.95 eV to 2.48 eV (Table 1). A similar trend is observed for series CTF-2 Suzuki to CTF-4 Suzuki, but these materials fall within a much narrower range (2.93 eV–2.85 eV). As such, the synthesis route seems to have an important impact on the photophysical properties of the materials, possibly due to differences in defects within the material and end-groups. In both series, the material with four-phenylene spacers (CTF-4 and CTF-4 Suzuki) is the most red-shifted and has the smallest optical gap (see Fig. 3).

All materials are weakly fluorescent upon excitation at 280 nm and show two characteristic maxima (Fig. S-5 and Fig. S-6, ESI). The maxima fall between 367 and 374 nm for the first peak and 448 and 476 nm for the second peak. No coherent trends can be found within either series of polymers, and the observed Stokes' shifts are small, possibly an indication of rigidity.

We tested all materials for photocatalytic hydrogen evolution from water in the presence of triethanolamine (TEOA, 20 vol %) acting as a sacrificial hole-scavenger [32,34,36]. For improved performance, the materials were loaded with 3 wt % platinum as

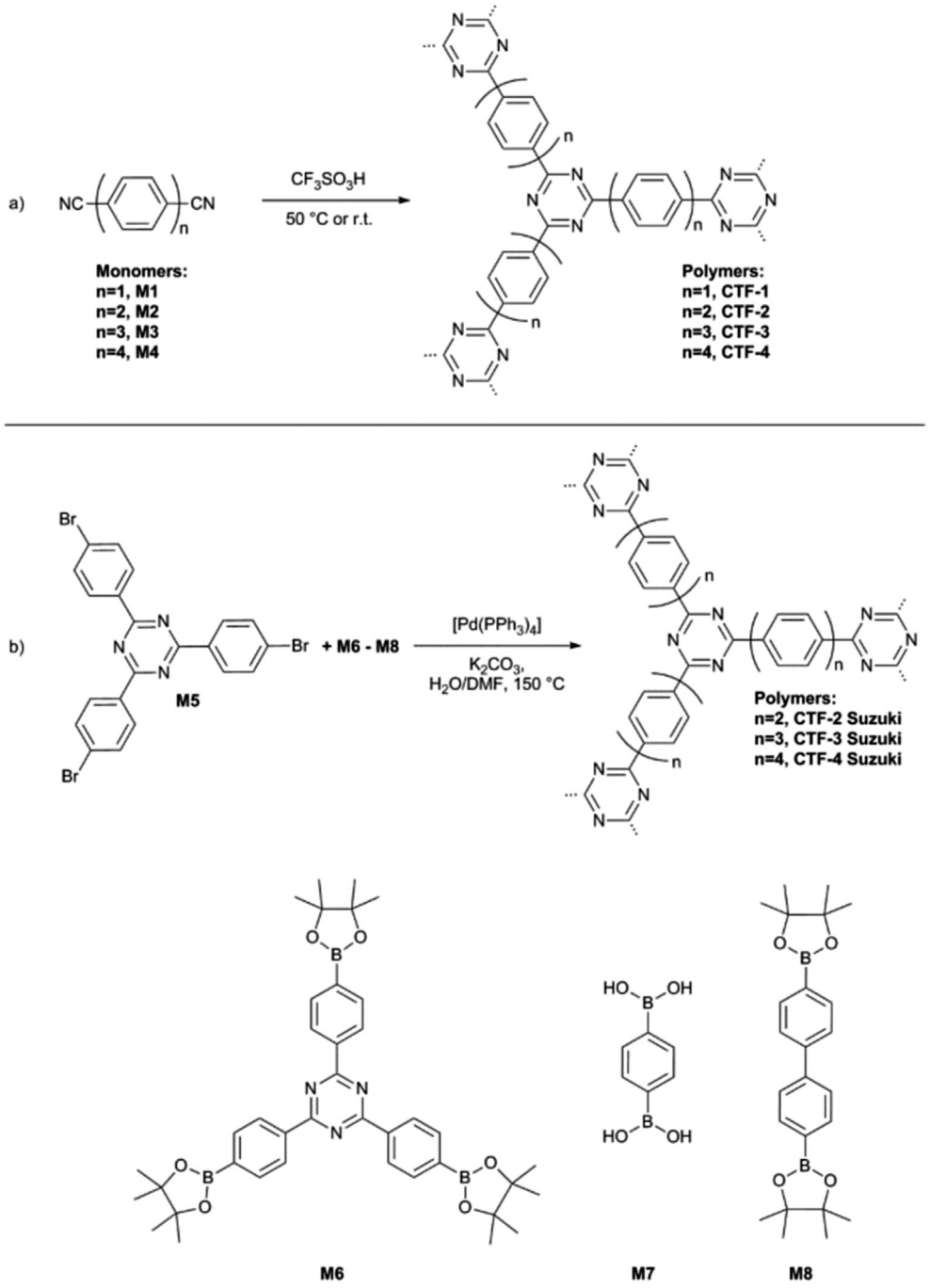

Fig. 1. Synthetic scheme for covalent triazine-based frameworks (CTFs) showing their representative repeating units: a) Trifluoromethanesulfonic acid catalyzed cyclotrimerization and b) Suzuki-Miyaura type polycondensation. Note that these simplified schematic representations do not show the defects and end-groups that will be present in these amorphous, porous networks.

the co-catalyst by *in situ* photodeposition of H_2PtCl_6 [24,36,46]. For CTF-2, Pt particles with diameters in the range of 17–33 μm were observed (Fig. S-34, ESI). All materials, with the exception of CTF-4 and CTF-4 Suzuki, were found to produce hydrogen under visible-light irradiation (>420 nm). The hydrogen evolution rates of all as-synthesized CTF samples were low, as the polymer powders were macroscopic flakes that were only poorly dispersible in the aqueous mixture (Fig. S-35, ESI). These issues were solved by ball milling the samples and we obtained hydrogen evolution rates of 35 μmol g^{-1} h^{-1} for CTF-1, 296 μmol g^{-1} h^{-1} for CTF-2, and 45 μmol g^{-1} h^{-1} for CTF-3 under >420 nm irradiation. When the materials were synthesized *via* Pd(0)-cross coupling reaction, slightly lower photocatalytic activities for the analogous polymers CTF-2 Suzuki (265 μmol g^{-1} h^{-1}) and CTF-3 Suzuki (44 μmol g^{-1} h^{-1}) were found when tested in the presence of the platinum co-catalyst, although these differences are probably smaller than the reproducibility of these measurements. These CTF materials show lower, but still significant, activity even without added platinum co-catalyst; *e.g.* for CTF-2 Suzuki, the hydrogen evolution rate drops from 265 μmol g^{-1} h^{-1} with platinum co-catalyst to 121 μmol g^{-1} h^{-1} without added platinum (Fig. 19, ESI). As for organic solar cells [47–49], residual palladium is

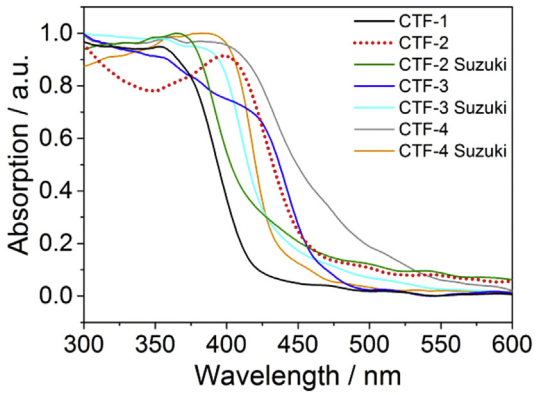

Fig. 2. UV-Visible reflectance spectra of the polymers measured in the solid-state (normalized intensities).

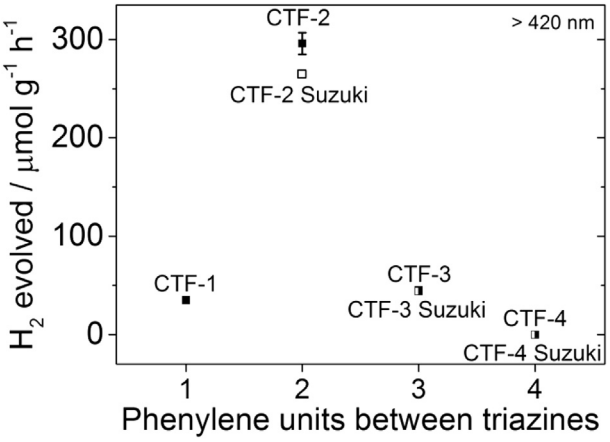

Fig. 3. The photocatalytic hydrogen evolution rates (HER) are correlated with the length of the phenylene spacers between the triazine units (open symbols: CTF Suzuki, filled symbols: acid-catalyzed CTF). Each measurement was performed with 25 mg ball milled catalyst from water/triethanolamine mixtures (90 vol %/10 vol %) with 3 wt % platinum co-catalyst under visible-light irradiation (λ > 420 nm). The error bars for CTF-1, CTF-2 Suzuki, CTF-3 and CTF-3 Suzuki are below 5 µmol g^{-1} h^{-1}.

found as particles in these polymers, which have been suggested to act as co-catalysts in a recent report on photocatalytically active CMPs [24]. Palladium was also reported to be active in conjunction with g-C_3N_4 [50], albeit with a lower activity than platinum, in line with the trends observed here. In contrast, CTF-2 does not produce hydrogen in absence of the Pt co-catalyst from water/

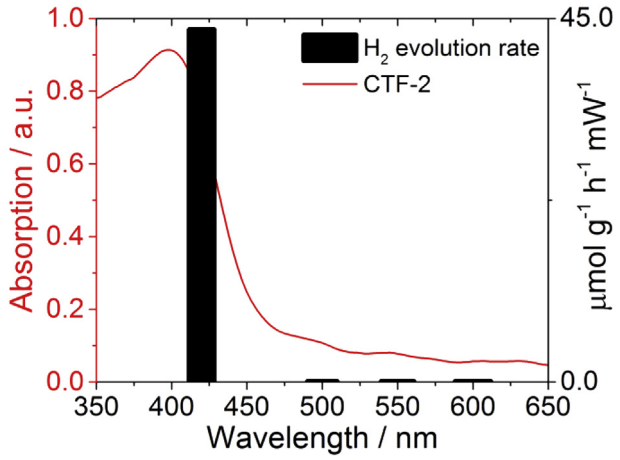

Fig. 4. Wavelength dependency of the photocatalytic hydrogen evolution for CTF-2 ball milled using band-pass filters (420 nm, 500 nm, 550 nm and 600 nm ± 10 nm, FWHM). The suspension of the polymer in water with 20 vol % of triethanolamine and 3 wt % Pt was measured in a quartz cuvette with an area of 7.8 cm^2 for an illumination time of at least 5 h.

triethanolamine solution (Fig. S-19, ESI). No hydrogen could be detected from suspensions of CTF-2 in water (Fig. S-20, ESI), CTF-2 water platinum particle suspensions (Fig. S-20, ESI), and from water/triethanolamine solutions in the absence of photocatalysts (Fig. S-21, ESI). The apparent quantum yield (AQY) [51] of CTF-2 was calculated to be 1.6% at 420 nm (±10 nm, FWHM, Fig. 4), which is higher than poly(*p*-phenylene) ($AQY_{420\ nm}$ = 0.4%) but lower than poly(dibenzo[*b*,*d*]thiophene sulfone-*co*-phenylene) ($AQY_{420\ nm}$ = 7.2%) [26]. No photocatalytic activity was found under 600 nm, 550 nm or 500 nm illumination using band-pass filters, indicating that the hydrogen evolution is indeed a photocatalytic process. Furthermore, photocurrents were measured for CTF-1, CTF-2, and CTF-4 under >420 nm illumination, these show that the process is indeed photocatalytic (Fig. S-29, ESI).

The photocatalytic stability of CTF-2 was also tested under 1 Sun illumination (using an ABA-certified solar-simulator as the light source) for a total of 38 h. The performance slightly decreased after three hours, but stabilized to a constant evolution rate of 526 µmol g^{-1} h^{-1}. After 38 h, the polymer evolved more hydrogen than present in the material, ruling out decomposition of the polymer as the source of hydrogen.

Calculations were performed using our established computational approach [52,53] based around density functional theory calculations on cluster models of the CTF materials (Fig. S-44, ESI). The results of these calculations are presented in Fig. 5 and suggest

Table 1
Photophysical properties and hydrogen evolution rates (HERs) for the polymer photocatalysts.

Polymer	Optical gap[a]/eV	λ_{max}[b]/nm, eV	Predicted λ_{max}[c]/eV	λ_{em}[d]/nm	HER >420 nm[e]/µmol g^{-1} h^{-1}
CTF-1	2.95	354, 3.50	3.85	374, 469	35 ± 1
CTF-2	2.73	398, 3.12	3.49	367, 448	296 ± 11
CTF-3	2.62	404, 3.07	3.27	372, 468	45 ± 1
CTF-4	2.48	382, 3.25	3.17	372, 476	0[f]
CTF-2 Suzuki	2.93	365, 3.40	-[g]	373, 466	265 ± 5
CTF-3 Suzuki	2.88	377, 3.29	-[g]	370, 452	44 ± 2
CTF-4 Suzuki	2.85	387, 3.20	-[g]	371, 467	0[f]

[a] The optical gap was calculated from the on-set of absorption in the solid-state UV-vis spectrum.
[b] λ_{max} was determined from the peak maximum of the most red-shifted peak in the solid state UV-vis spectrum.
[c] The predicted λ_{max} were obtained from TD-B3LYP calculations on LT_2L_4 cluster models of the CTFs (L = linker, T = triazine).
[d] λ_{em} was recorded at λ_{ex} = 280 nm (Fig. S-5 and Fig. S-6, ESI).
[e] The hydrogen evolution rate (HER) was measured with 25 mg of the ball milled samples in water, 20% triethanolamine and 3 wt % platinum as a co-catalyst.
[f] No hydrogen evolved during a typical 5 h run.
[g] See CTF-2 to CTF-4 for predicted values.

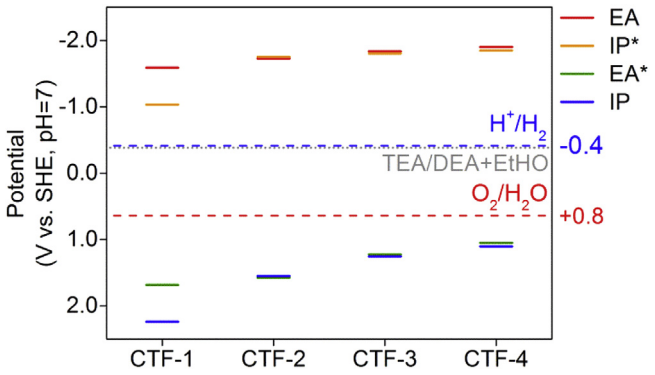

Fig. 5. Predicted values of the IP*, EA*, IP and EA standard reduction potentials of CTF-1 to CTF-4 for expanded cluster models (Fig. S-44, ESI) *vs.* the calculated standard reduction potentials of proton reduction (blue line), water oxidation (red line) and triethylamine oxidation (grey line). All potentials are calculated for pH = 7 and a relative dielectric permittivity of 80.1 (water). (For interpretation of the references to colour in this figure legend, the reader is referred to the web version of this article.)

that the thermodynamic driving force for proton reduction is similar for all materials (difference between EA; red line, and the proton reduction potential; blue line). However, the predicted driving force for the oxidation of the sacrificial hole-scavenger decreases within the series from CTF-1 to CTF-4. In Fig. 5 the oxidation of triethylamine to diethylamine and acetaldehyde is shown (difference between IP; blue line, and the triethylamine oxidation potential; grey line), but similar conclusions can be drawn for any sacrificial hole-scavenger as the oxidation potential of a sacrificial hole-scavenger is independent of the material studied. Results for the excited state EA* and IP* potentials are discussed in more detail in the supporting information.

In comparison to our measurements, this at first appears to be inconsistent with the fact that CTF-2 is the most active material, especially under illumination with a solar simulator. The photocatalytic activity of these materials is, however, the product of several properties, such as the driving force for both half-reactions and the number of photons absorbed, as well as the ease of charge transport [54]. We therefore investigated in more detail the spectral effects on the observed activity for CTF-1 and CTF-2.

Going from >420 nm irradiation to broad spectrum illumination with a Xe lamp and a >295 nm cut-off filter (Fig. S-24, ESI) leads to an increase in the hydrogen evolution rate from 35 μmol g^{-1} h^{-1} to 94 μmol g^{-1} h^{-1} for CTF-1 and from 296 μmol g^{-1} h^{-1} to 374 μmol g^{-1} h^{-1} for CTF-2 (Fig. S-11, ESI). This increased activity is caused by absorption of UV-photons, showing that CTF-1 is more active under >295 nm UV-light and has limited absorption of visible light photons. We also compared the activity of CTF-1 and CTF-2 when illuminated with exclusively UV light using a U-340 band-pass filter (260–390 nm, see Fig. S-24, ESI for transmission characteristics). Under these conditions, CTF-1 slightly outperforms CTF-2, evolving 118 μmol g^{-1} h^{-1} *vs.* 111 μmol g^{-1} h^{-1}, respectively. Considering all these measurements and our calculations, it appears that the experimentally observed maximum in visible light activity in the series for CTF-2 is the result of a trade-off between the total amount of light absorbed and the thermodynamic driving force for the oxidation reaction. Along the series from CTF-1 to CTF-4, the amount of light absorbed increases as the optical gap decreases, while the driving force for the oxidation of a sacrificial hole-scavenger, *i.e.* triethanolamine or triethylamine, decreases within the series.

Calculations also predict that CTF-4 should evolve hydrogen in the presence of triethylamine, which is in contrast to the observed lack of activity in experiment when using triethanolamine as sacrificial hole-scavenger. As in previous studies [21,23,26], we therefore tested the materials in water/triethylamine/methanol mixtures under >420 nm illumination. The addition of methanol has been found previously to act as a co-solvent, thus avoiding phase separation between water and triethylamine [23,26], and also to improve surface wettability for hydrophobic polymers. For ball milled CTF-2, the hydrogen evolution rates under visible-light are slightly higher when using water/methanol/triethylamine mixtures compared to water/triethanolamine mixtures (358 *vs.* 296 μmol g^{-1} h^{-1}). For CTF-1 and CTF-3, the hydrogen evolution rates nearly double from 35 to 66 μmol g^{-1} h^{-1} and from 45 to 79 μmol g^{-1} h^{-1}, respectively, with the water/triethylamine/methanol system. More importantly, this mixture leads to a low hydrogen evolution rate of 24 μmol g^{-1} h^{-1} for CTF-4, in line with our prediction that this polymer should be able to evolve hydrogen. The fact that no visual improvement could be observed in polymer dispersibility in water/methanol/triethylamine mixtures in comparison to water/triethanolamine mixtures suggests that the increased hydrogen evolution activity for CTFs might result from the easier oxidation of triethylamine compared to triethanolamine.

4. Conclusions

The photocatalytic hydrogen evolution rates of seven CTFs using sacrificial hole-scavengers were studied and the results were compared with the predictions of (TD)-DFT calculations. The photocatalytic activity is not significantly different for materials synthesized using catalyzed trimerization or Suzuki-Miyaura type polycondensation, despite some differences in the optical properties. In both series of polymers, UV-vis spectra show a trend of decreasing optical gaps as the phenylene spacer length increases. CTF-2 showed the highest hydrogen evolution rate under visible light using triethanolamine as sacrificial hole-scavenger and this shows that microporosity does not preclude efficient photocatalytic water reduction. This is noteworthy, since in principle microporosity might reduce charge transport rates in the solid state, which could offset gains in mass transport. Under UV light, the activity of CTF-2 increased slightly, whereas CTF-1 evolved nearly twice the amount of hydrogen in comparison to the irradiation >420 nm. These results suggest that the absorption of visible photons is limited in CTF-1 and therefore decreases its hydrogen evolution rate under these conditions. This observation is supported by calculations predicting CTF-1 to have the largest thermodynamic driving force in the series from CTF-1 to CTF-4. In general, the trend in the activity of the CTF series and the origin of the maximum in hydrogen evolution rate for CTF-2 appears to be a combination of the thermodynamic driving force and the optical gap, highlighting how the activity of a material can be controlled by structural property tuning. Residual palladium in the Suzuki-Miyaura derived materials seems to act as a co-catalyst, however, the photocatalytic activity can be further improved by the addition of platinum. Finally, CTF-2 shows a stable hydrogen evolution rate under simulated solar light for at least 38 h, evolving more hydrogen than present in the material and showcasing the stability of the material.

Acknowledgements

We thank the Engineering and Physical Sciences Research Council for financial support under Grant EP/N004884/1. M.A.Z. furthermore acknowledge EPSRC for a Career Acceleration Fellowship (Grant EP/I004424/1). We acknowledge computational time on the EPSRC National Service for Computational Chemistry Software. C.B.M. thanks Rob Clowes for help with sorption measurements.

Appendix A. Supplementary data

Supplementary data related to this article can be found at http://dx.doi.org/10.1016/j.polymer.2017.04.017.

References

[1] X. Chen, S. Shen, L. Guo, S.S. Mao, Semiconductor-based photocatalytic hydrogen generation, Chem. Rev. 110 (2010) 6503–6570.
[2] A. Kudo, Y. Miseki, Heterogeneous photocatalyst materials for water splitting, Chem. Soc. Rev. 38 (2009) 253–278.
[3] L. Yang, H. Zhou, T. Fan, D. Zhang, Semiconductor photocatalysts for water oxidation: current status and challenges, Phys. Chem. Chem. Phys. 16 (2014) 6810–6826.
[4] G. Zhang, Z.-A. Lan, X. Wang, Conjugated polymers: catalysts for photocatalytic hydrogen evolution, Angew. Chem. Int. Ed. 55 (2016) 15712–15727.
[5] X. Wang, K. Maeda, A. Thomas, K. Takanabe, G. Xin, J.M. Carlsson, K. Domen, M. Antonietti, A metal-free polymeric photocatalyst for hydrogen production from water under visible light, Nat. Mater. 8 (2009) 76–80.
[6] Y. Zheng, L. Lin, B. Wang, X. Wang, Graphitic carbon nitride polymers toward sustainable photoredox catalysis, Angew. Chem. Int. Ed. 54 (2015) 12868–12884.
[7] S. Cao, J. Low, J. Yu, M. Jaroniec, Polymeric photocatalysts based on graphitic carbon nitride, Adv. Mater. 27 (2015) 2150–2176.
[8] V.W.-H. Lau, M.B. Mesch, V. Duppel, V. Blum, J. Senker, B.V. Lotsch, Low-molecular-weight carbon nitrides for solar hydrogen evolution, J. Am. Chem. Soc. 137 (2015) 1064–1072.
[9] W.-J. Ong, L.-L. Tan, Y.H. Ng, S.-T. Yong, S.-P. Chai, Graphitic carbon nitride (g-C_3N_4)-Based photocatalysts for artificial photosynthesis and environmental remediation: are we a step closer to achieving sustainability? Chem. Rev. 116 (2016) 7159–7329.
[10] S. Cao, J. Yu, g-C_3N_4-based photocatalysts for hydrogen generation, J. Phys. Chem. Lett. 5 (2014) 2101–2107.
[11] J. Liu, Y. Liu, N. Liu, Y. Han, X. Zhang, H. Huang, Y. Lifshitz, S.-T. Lee, J. Zhong, Z. Kang, Metal-free efficient photocatalyst for stable visible water splitting via a two-electron pathway, Science 347 (2015) 970–974.
[12] G. Zhang, Z.-A. Lan, L. Lin, S. Lin, X. Wang, Overall water splitting by Pt/g-C_3N_4 photocatalysts without using sacrificial agents, Chem. Sci. 7 (2016) 3062–3066.
[13] J. Zhang, X. Chen, K. Takanabe, K. Maeda, K. Domen, J.D. Epping, X. Fu, M. Antonietti, X. Wang, Synthesis of a carbon nitride structure for visible-light catalysis by copolymerization, Angew. Chem. Int. Ed. 49 (2010) 441–444.
[14] K. Schwinghammer, B. Tuffy, M.B. Mesch, E. Wirnhier, C. Martineau, F. Taulelle, W. Schnick, J. Senker, B.V. Lotsch, Triazine-based carbon nitrides for visible-light-driven hydrogen evolution, Angew. Chem. Int. Ed. 52 (2013) 2435–2439.
[15] J. Zhang, J. Sun, K. Maeda, K. Domen, P. Liu, M. Antonietti, X. Fu, X. Wang, Sulfur-mediated synthesis of carbon nitride: band-gap engineering and improved functions for photocatalysis, Energy Environ. Sci. 4 (2011) 675–678.
[16] S. Hu, F. Li, Z. Fan, F. Wang, Y. Zhao, Z. Lv, Band gap-tunable potassium doped graphitic carbon nitride with enhanced mineralization ability, Dalt. Trans. 44 (2015) 1084–1092.
[17] S. Yanagida, A. Kabumoto, K. Mizumoto, C. Pac, K. Yoshino, Poly(p-phenylene)-catalysed photoreduction of water to hydrogen, J. Chem. Soc. Chem. Commun. (1985) 474–475.
[18] T. Shibata, A. Kabumoto, T. Shiragami, O. Ishitani, C. Pac, S. Yanagida, Novel visible-light-driven photocatalyst. Poly(p-phenylene)-Catalyzed photoreductions of water, carbonyl compounds, and olefins, J. Phys. Chem. 94 (1990) 2068–2076.
[19] S. Matsuoka, H. Fujii, T. Yamada, C. Pac, A. Ishida, S. Takamuku, M. Kusaba, N. Nakashima, S. Yanagida, Photocatalysis of oligo(p-phenylenes). Photoreductive production of hydrogen and ethanol in aqueous triethylamine, J. Phys. Chem. 95 (1991) 5802–5808.
[20] S. Matsuoka, T. Kohzuki, Y. Kuwana, A. Nakamura, S. Yanagida, Visible-light-induced photocatalysis of poly(pyridine-2,5-diyl). Photoreduction of water, carbonyl compounds and alkenes with triethylamine, J. Chem. Soc. Perkin Trans. 2 (1992) 679–685.
[21] R.S. Sprick, J.-X. Jiang, B. Bonillo, S. Ren, T. Ratvijitvech, P. Guiglion, M.A. Zwijnenburg, D.J. Adams, A.I. Cooper, Tunable organic photocatalysts for visible-light-driven hydrogen evolution, J. Am. Chem. Soc. 137 (2015) 3265–3270.
[22] V.S. Vyas, B.V. Lotsch, Organic polymers form fuel from water, Nature 521 (2015) 41–42.
[23] R.S. Sprick, B. Bonillo, M. Sachs, R. Clowes, J.R. Durrant, D.J. Adams, A.I. Cooper, Extended conjugated microporous polymers for photocatalytic hydrogen evolution from water, Chem. Commun. 52 (2016) 10008–10011.
[24] L. Li, Z. Cai, Q. Wu, W.-Y. Lo, N. Zhang, L.X. Chen, L. Yu, Rational design of porous conjugated polymers and roles of residual palladium for photocatalytic hydrogen production, J. Am. Chem. Soc. 138 (2016) 7681–7686.
[25] L. Li, W.-Y. Lo, Z. Cai, N. Zhang, L. Yu, Donor–acceptor porous conjugated polymers for photocatalytic hydrogen production: the importance of acceptor comonomer, Macromolecules 49 (2016) 6903–6909.
[26] R.S. Sprick, B. Bonillo, R. Clowes, P. Guiglion, N.J. Brownbill, B.J. Slater, F. Blanc, M.A. Zwijnenburg, D.J. Adams, A.I. Cooper, Visible light-driven hydrogen evolution using planarized conjugated polymer photocatalysts, Angew. Chem. Int. Ed. 128 (2016) 1824–1828.
[27] C. Yang, B.C. Ma, L. Zhang, S. Lin, S. Ghasimi, K. Landfester, K.A.I. Zhang, X. Wang, Molecular engineering of conjugated polybenzothiadiazoles for enhanced hydrogen production by photosynthesis, Angew. Chem. Int. Ed. 55 (2016) 9348–9352.
[28] L. Wang, R. Fernández-Terán, L. Zhang, D.L.A. Fernandes, L. Tian, H. Chen, H. Tian, Organic polymer dots as photocatalyst for visible light-driven hydrogen generation, Angew. Chem. Int. Ed. 55 (2016) 12306–12310.
[29] P. Kuhn, M. Antonietti, A. Thomas, Porous, covalent triazine-based frameworks prepared by ionothermal synthesis, Angew. Chem. Int. Ed. 47 (2008) 3450–3453.
[30] M.J. Bojdys, J. Jeromenok, A. Thomas, M. Antonietti, Rational extension of the family of layered, covalent, triazine-based frameworks with regular porosity, Adv. Mater. 22 (2010) 2202–2205.
[31] S. Kuecken, J. Schmidt, L. Zhi, A. Thomas, Conversion of amorphous polymer networks to covalent organic frameworks under ionothermal conditions: a facile synthesis route for covalent triazine frameworks, J. Mater. Chem. A 3 (2015) 24422–24427.
[32] K. Schwinghammer, S. Hug, M.B. Mesch, J. Senker, B.V. Lotsch, Phenyl-triazine oligomers for light-driven hydrogen evolution, Energy Environ. Sci. 8 (2015) 3345–3353.
[33] L. Stegbauer, K. Schwinghammer, B.V. Lotsch, A hydrazone-based covalent organic framework for photocatalytic hydrogen production, Chem. Sci. 5 (2014) 2789–2793.
[34] V.S. Vyas, F. Haase, L. Stegbauer, G. Savasci, F. Podjaski, C. Ochsenfeld, B.V. Lotsch, A tunable azine covalent organic framework platform for visible light-induced hydrogen generation, Nat. Commun. 6 (2015) 8508.
[35] A. Bhunia, D. Esquivel, S. Dey, R. Fernández-Terán, Y. Goto, S. Inagaki, P. Van Der Voort, C. Janiak, A photoluminescent covalent triazine framework: CO_2 adsorption, light-driven hydrogen evolution and sensing of nitroaromatics, J. Mater. Chem. A 4 (2016) 13450–13457.
[36] J. Bi, W. Fang, L. Li, J. Wang, S. Liang, Y. He, M. Liu, L. Wu, Covalent triazine-based frameworks as visible light photocatalysts for the splitting of water, Macromol. Rapid Commun. 36 (2015) 1799–1805.
[37] M.A. Ismail, R.K. Arafa, R. Brun, T. Wenzler, Y. Miao, W.D. Wilson, C. Generaux, A. Bridges, J.E. Hall, D.W. Boykin, Synthesis, DNA affinity, and antiprotozoal activity of linear dications: terphenyl diamidines and analogues, J. Med. Chem. 49 (2006) 5324–5332.
[38] M. Schiek, K. Al-Shamery, A. Lützen, Synthesis of Symmetrically and Unsymmetrically *para*-Functionalized *p*-Quaterphenylenes, Synthesis 4 (2007) 0613–0621.
[39] F. Furche, R. Ahlrichs, C. Hättig, W. Klopper, M. Sierka, F. Weigend, Turbomole, WIREs Comput. Mol. Sci. 4 (2014) 91–100.
[40] A.D. Becke, Density-functional thermochemistry. III. The role of exact exchange, J. Chem. Phys. 98 (1993) 5648–5652.
[41] P.J. Stephens, F.J. Devlin, C.F. Chabalowski, M.J. Frisch, *Ab initio* calculation of vibrational absorption and circular dichroism spectra using density functional force fields, J. Phys. Chem. 98 (1994) 11623–11627.
[42] A. Klamt, G. Schüürmann, COSMO: a new approach to dielectric screening in solvents with explicit expressions for the screening energy and its gradient, J. Chem. Soc. Perkin Trans. 2 (1993) 799–805.
[43] S. Ren, M.J. Bojdys, R. Dawson, A. Laybourn, Y.Z. Khimyak, D.J. Adams, A.I. Cooper, Porous, fluorescent, covalent triazine-based frameworks via room-temperature and microwave-assisted synthesis, Adv. Mater. 24 (2012) 2357–2361.
[44] C.R. DeBlase, W.R. Dichtel, Moving beyond boron: the emergence of new linkage chemistries in covalent organic frameworks, Macromolecules 49 (2016) 5297–5305.
[45] Y. Zeng, R. Zou, Z. Luo, H. Zhang, X. Yao, X. Ma, R. Zou, Y. Zhao, Covalent organic frameworks formed with two types of covalent bonds based on orthogonal reactions, J. Am. Chem. Soc. 137 (2015) 1020–1023.
[46] M.G. Schwab, M. Hamburger, X. Feng, J. Shu, H.W. Spiess, X. Wang, M. Antonietti, K. Müllen, Photocatalytic hydrogen evolution through fully conjugated poly(azomethine) networks, Chem. Commun. 46 (2010) 8932–8934.
[47] K.T. Nielsen, K. Bechgaard, F.C. Krebs, Removal of palladium nanoparticles from polymer materials, Macromolecules 38 (2005) 658–659.
[48] M.P. Nikiforov, B. Lai, W. Chen, S. Chen, R.D. Schaller, J. Strzalka, J. Maser, S.B. Darling, Detection and role of trace impurities in high-performance organic solar cells, Energy Environ. Sci. 6 (2013) 1513–1520.
[49] C. Bracher, H. Yi, N.W. Scarratt, R. Masters, A.J. Pearson, C. Rodenburg, A. Iraqi, D.G. Lidzey, The effect of residual palladium catalyst on the performance and stability of PCDTBT:PC70BM organic solar cells, Org. Electron 27 (2015) 266–273.
[50] K. Maeda, X. Wang, Y. Nishihara, D. Lu, M. Antonietti, K. Domen, Photocatalytic activities of graphitic carbon nitride powder for water reduction and oxidation under visible light, J. Phys. Chem. C 113 (2009) 4940–4947.
[51] C.A. Caputo, M.A. Gross, V.W. Lau, C. Cavazza, B.V. Lotsch, E. Reisner, Photocatalytic hydrogen production using polymeric carbon nitride with a

hydrogenase and a bioinspired synthetic Ni catalyst, Angew. Chem. Int. Ed. 53 (2014) 11538–11542.
[52] P. Guiglion, C. Butchosa, M.A. Zwijnenburg, Polymer photocatalysts for water splitting: insights from computational modeling, Macromol. Chem. Phys. 217 (2016) 344–353.
[53] C. Butchosa, P. Guiglion, M.A. Zwijnenburg, Carbon nitride photocatalysts for water splitting: a computational perspective, J. Phys. Chem. C 118 (2014) 24833–24842.
[54] P. Guiglion, E. Berardo, C. Butchosa, M.C.C. Wobbe, M.A. Zwijnenburg, Modelling materials for solar fuel synthesis by artificial photosynthesis; predicting the optical, electronic and redox properties of photocatalysts, J. Phys.: Condens. Matter 28 (2016) 074001.